

EFFECTS OF FAR-FIELD SHEARING DEFORMATION ON FRACTURING AROUND AN UNDERGROUND OPENING

By M. K. Larson, B. G. White, and S. R. Iverson
*Spokane Research Laboratory, National Institute for Occupational Safety and Health,
Spokane, WA*

ABSTRACT

Researchers at the National Institute for Occupational Safety and Health (NIOSH) are investigating the causes and mechanisms of roof failure in underground mines. It is expected that a better understanding of these causes and mechanisms will lead to better layout and support designs that will help prevent accidents and fatalities associated with fall of ground. Two numerical experiments were conducted by NIOSH researchers using the Fast Lagrangian Analysis of Continua (FLAC) computer modeling program with a strain-softening continuum to simulate fracture zones. Two models, one of a round hole in a plate and one of a rectangular opening, were constructed and boundary conditions were applied to simulate far-field shear. The Particle Flow Code in Two Dimensions (PFC^{2D}) computer program was used to look at the effects of far-field shear in generating fractures around an underground opening, but these models are preliminary until boundary conditions, strengths, and stiffnesses are matched to the FLAC models. Results showed that shear zones propagated from the opposite corners of openings in directions that appeared to be determined by opening shape and far-field stress. Tensile failures also formed and extended away from these shear zones. The consistent direction of shear deformation with respect to far-field shear provides a plausible explanation for preferred directions of shear as seen in geologic environments.

INTRODUCTION

Fairhurst and Cook (1966) proposed a roof-rib failure mechanism in which parallel, stress-induced microcracks form parallel to the roof or rib line. Stress around the opening causes these microcracks to increase in length. The length of these fractures decreases with distance from the opening, and, in the event of a roof fall or rock burst, their ends define a limit of breakage that is concave to the surface. Diederichs (2003) illustrates a zone of fractures with the same geometry as fractures described by Fairhurst and Cook (1966). However, White (2002) examined failure around an underground opening and concluded that the closely spaced fractures describe by these authors did not extend through the entire volume of fallen rock, but were limited to near the periphery of the breakout. Other examples are cited in White et al. (2003) that support this assertion.

Terrill and VandeKraats (1997) observed similar features in a salt mine after the fractured roof was excavated by a roadheader. They noted that fractures first formed near corners, and then

either took the form of a fault that angled upward toward the centerline of the roof or more often, a zone of en echelon fractures that angled over the opening. Zones of both faults and en echelon fractures displayed a component of slip. The alternating appearance of faults and en echelon fractures and their similar displacements suggested that both structures were closely related, an idea that was also considered by Peng and Johnson (1972).

Using the observations of Terrill and VandeKraats (1997), White et al. (2003) concluded that a fundamental pattern of fracturing around rectangular underground openings involves dilatatory shear zones that originate near the corners of openings and propagate obliquely away from these corners to intersect the vertical centerline of the opening, as seen in figure 1.



Figure 1.— Representative cross section showing fracture patterns in halite roof (modified from Terrill and VandeKraats 1997: figure 6).

Larson et al. (1995), Larson and Maleki (1996), and Larson (2003) describe roof failures in the roof of a coal mine in which the immediate rock above the coal seam was a carbonaceous mudstone containing weak bedding planes. Failure typically occurred over time near the upper corner on the downdip side of the roof, creating a zone of failure. This failure zone then began to extend over the entry. Larson et al. (1995) and Larson (2003) surmised that, over time, much of the deformation might become concentrated along the weak planes as a result of far-field shear driving forces along these planes. A dip of 16° at one of the two sites studied added credence to this hypothesis. The question arises as to whether typical far-field shear deformation resulting from shear stress or shear ride can cause zones of shear and tensile fracturing to extend in a preferred direction (for example, fracturing on only one side of an opening).

PREVIOUS MODELS

White et al. (2003, 2004) conducted numerical experiments with two computer modeling codes: Fast Lagrangian Analysis of Continua (FLAC) (Itasca Consulting Group, 1993) and Particle Flow Code (PFC^{2D}) (Itasca Consulting Group, 1999). Continuum modeling with FLAC using very small elements under far-field compressive stresses of 68.95 MPa (10,000 psi) horizontally and 34.47 MPa (5,000 psi) vertically identified a small but significant zone of tension near each corner of the roof following excavation of the opening. The effects of a crack

parallel to the opening were simulated by removing an element at that position and extending the “crack” (figure 2). The result was that the tension zone migrated, staying above and near the end of the crack, but peak tension decreased in magnitude. This pattern suggests that another crack might form above and be offset from the first crack and that propagation of such a system of cracks would eventually stop.

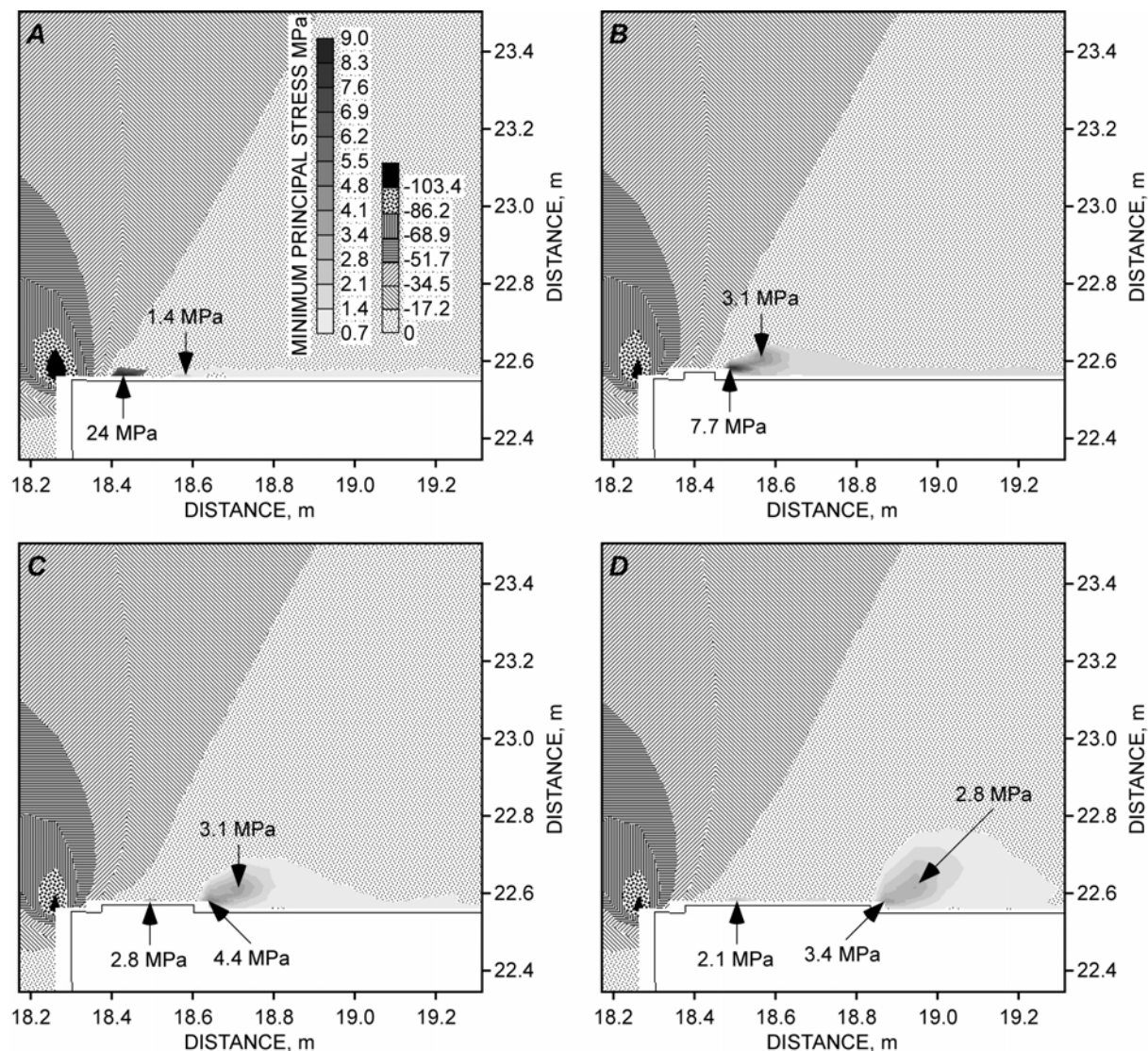


Figure 2.—Portion of FLAC model showing least principal stress near corner of rectangular opening using stress conditions and rock properties approximating those of the Coeur d’Alene Mining District. Untextured pattern along edge of opening reflects tension. A, Initial model. Tension reaches 24 MPa (3,480 psi) near corner, but 1.4 MPa (200 psi) maximum along edge of roof farther from corner. B, C, D, Least principal stress for simulated fracture created by removing progressively longer row of narrow elements. B, Removal of element containing highest stress in A. A region of tension extends diagonally upward to second site of concentrated tension. C, D, Third and fourth tension sites revealed as simulated fracture extends to right, tensile regime expands, and tension sites at end of simulated fracture move with progressive extension of fracture (White et al. 2004:figure 3).

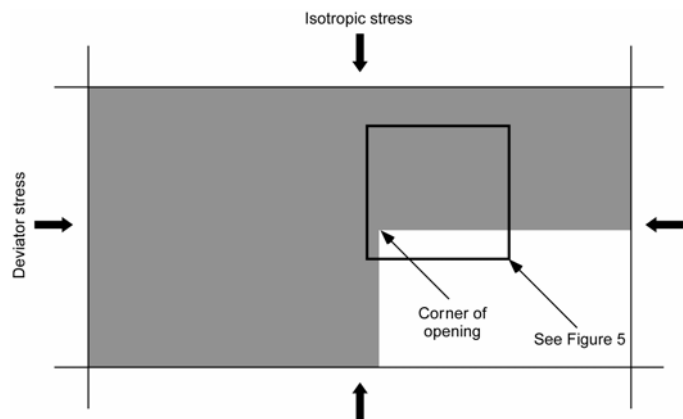


Figure 3.—PFC model in which margins of rectangular block of particles are loaded and a rectangular area excavated to simulate cross section of corner of mine opening. Horizontal load is gradually increased so progressive failure can be observed (White et al. 2004:figure 4).

Discrete-element modeling with two-dimensional particles using PFC^{2D}, in which an isotropic stress was applied to all walls (or external boundaries), was done next. The opening was then excavated and vertical load increased (figure 3). Figure 4 shows the formation of several en echelon cracks. While boundary conditions do not represent the effects of excavation, they may represent further loading of an opening because of nearby mining.

While both the FLAC and PFC^{2D} modeling experiments showed a possible cause for the initial formation of en echelon zones and the possibility that additional loading could cause propagation of faults or en echelon fractures, it was not

clear what caused the extension of such fracture zones in the absence of loading (that is, fracturing resulting from mining of the opening) and what the mode of failure was. In the case of the coal mine described, far-field shear ride is a likely cause. The rest of this paper examines the effects of far-field shearing on fracturing and identifies modes of failure and where failure occurs. It is a work in progress with results to date presented.

NUMERICAL EXPERIMENTS

Two experiments were conducted with FLAC models to examine the effects of far-field shearing. The first experiment used a round hole in a plate. The second experiment used a rectangular opening. One material type was used in each experiment. Material softening was used to simulate the loss of strength because of fracturing. Additional models were run with PFC^{2D} to examine the capabilities of particle modeling to simulate fracturing.

Hole-in-a-Plate Experiment

FLAC was used to examine fracturing caused by far-field shear around a circular opening. In this case, a mesh was mapped around a circular opening and joined to form a “glued” joint in the vertical plane down from the opening. Strain softening was used to simulate the effects of fracturing, and no dilation was assumed. Figure 5 shows graphically the assumed deterioration of (1) cohesion and friction with plastic shear displacement hardening/softening parameter e^{ps} and (2) tensile strength with plastic tensile displacement hardening/softening parameter e^{pt} . These are defined in incremental form as—

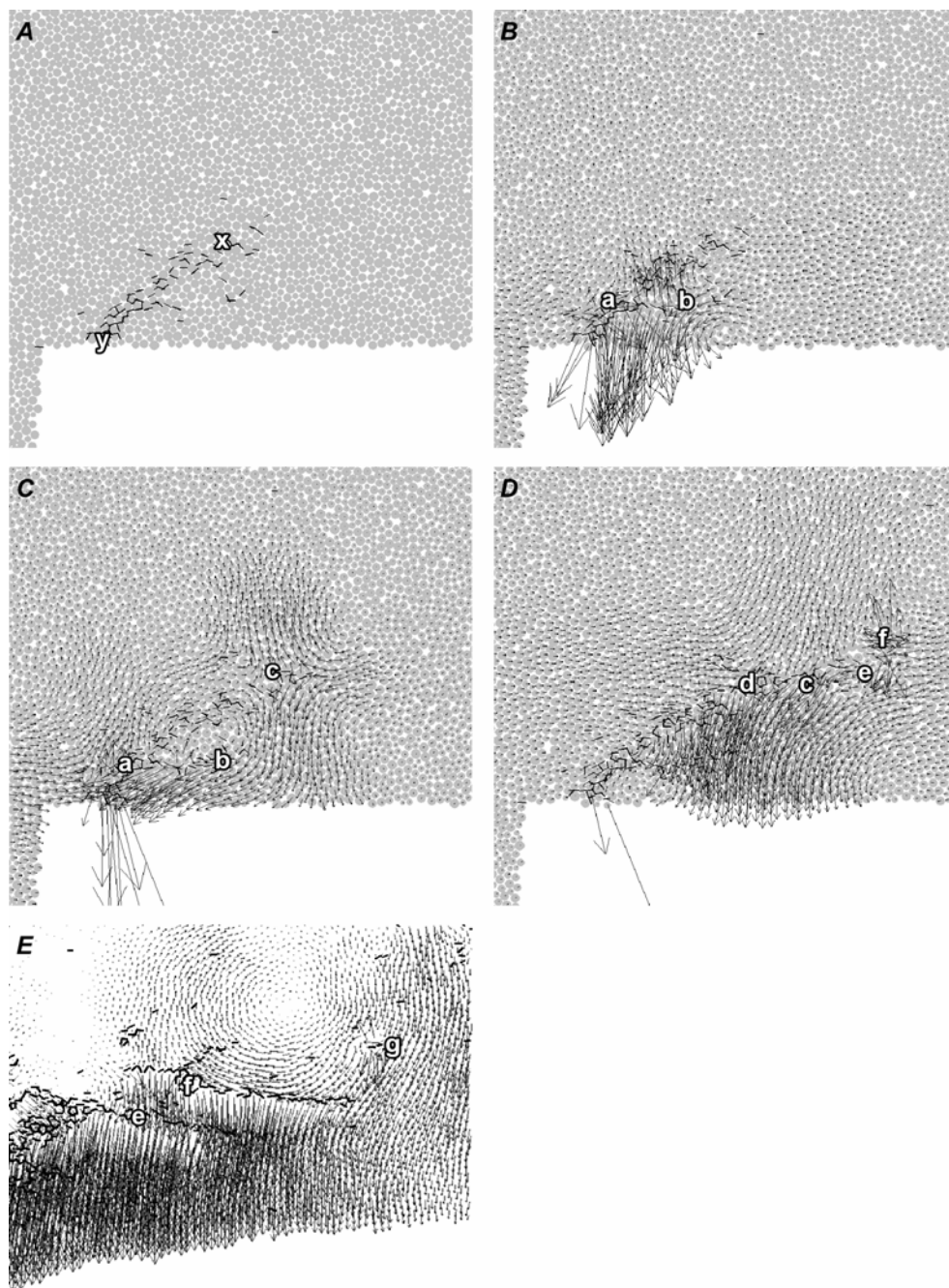


Figure 4.—Stages of progressive failure of square-corner model. *A*, Early stage of bond failure, identified as short lines. The first clustered failures occur at site X and spread downward; subsequent failures began and spread upward from site Y. Complete detachment along lower part of zone ultimately forms a fault. *B*, Velocity vectors (displacement from previous modeling step) during formation of wing crack a-b. Vectors indicate shear and dilational components along fault portion and also along wing crack. *C*, Velocity vectors as wing crack a-b reaches its fullest extent. A new cluster of failures (site of diverging vectors in offset position c) defines early stage of first en echelon fracture. Note scattered distribution of these early failures at this site. *D*, *E*, Velocity vectors indicate new en echelon fracture d-c-e and sites of initiation of two subsequent en echelon fractures f and g. In *D*, fault zone propagates to fracture d-c-e and activates it as a wing crack. Each long extension fracture propagates through a series of individual bond failures at fracture tips. Particles not shown in *E* (White et al. 2004:figure 5).

$$\Delta e^{ps} = \left\{ \frac{1}{2} (\Delta e_1^{ps} - \Delta e_m^{ps})^2 + \frac{1}{2} (\Delta e_m^{ps})^2 + \frac{1}{2} (\Delta e_3^{ps} - \Delta e_m^{ps})^2 \right\}^{\frac{1}{2}} \quad (1)$$

and
$$\Delta e^{pt} = \Delta e_3^{pt}, \quad (2)$$

where Δe_1^{ps} and Δe_3^{ps} are the incremental maximum and minimum principal plastic shear strains, respectively, Δe_3^{pt} is the incremental minimum principal plastic tensile strain, and

$$\Delta e_m^{ps} = \frac{1}{3} (\Delta e_1^{ps} + \Delta e_3^{ps}). \quad (3)$$

The softening functions shown in figure 5 were chosen to represent (1) the immediate loss of tensile strength at the moment of fracturing, (2) a quick loss of cohesive strength, which occurs at a slower rate than does the loss of tensile strength, and (3) a gradual deterioration of friction to a residual value. Peak strength values were chosen to represent a moderate to strong sedimentary or igneous rock.

Localization and softening behavior are somewhat mesh-dependent (Rice 1976; Fakhimi and Fairhurst 1994). Fakhimi and Fairhurst (1994) used an idea from Bazant and Pijaudier-Cabot (1988) of a nonlocal continuum in which stress at a point is a function of a weighted average of strains near that point. Characteristic size of the averaging zone is an important issue (Bazant and Pijaudier-Cabot 1987), but experiments done by Zietlow and Labuz (1998) suggest that characteristic size is related to grain size and fabric of the rock. In this paper, FLAC models did not use a nonlocal continuum model.

However, mesh size was small (19.6 by 9.5 mm [0.77 by 0.37 in] near the opening) and therefore not much larger than the typical grain size of several rock types.

A vertical compressive stress of 41.37 MPa (6,000 psi) and a horizontal compressive stress of 20.68 MPa (3,000 psi) were applied to the boundaries. Before applying shear stress to the boundaries, some shear yielding occurred on the sides at the position of greatest tangential compressive stress (figure 6A). In addition, minimal tensile yielding occurred in the vertical plane at the bottom of the opening but not at the top, probably because of the presence of the “glued” joint at the bottom.

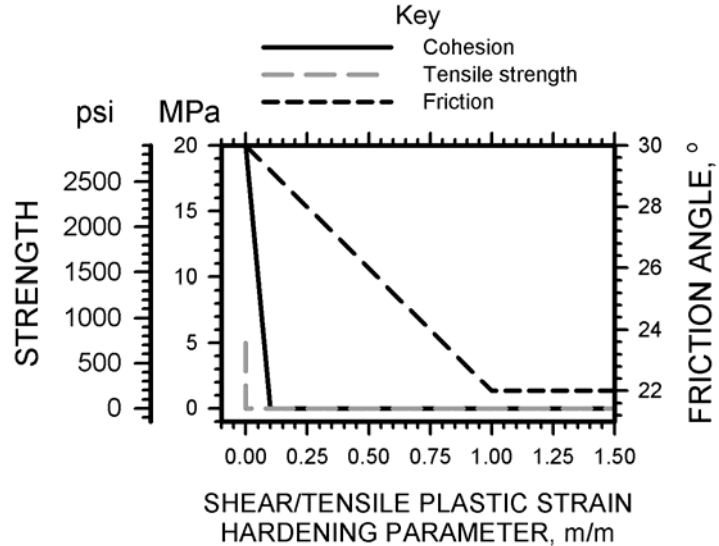


Figure 5.—Strength versus plastic strain functions assumed for FLAC experiments

A shear stress of 20.68 MPa (3,000 psi) was applied to the boundaries. Figure 6 shows model results. Figure 6B shows elements yielding at the end of the experiment and elements that had yielded in the past. Shear failure was largely localized in tight zones. Prominent shear failure zones extended from the upper right wall of the hole upward to the top boundary and from the lower left wall of the hole downward to the lower boundary. Figure 6C, D, and E shows the contours of cohesive, tensile, and frictional strengths, respectively. A less prominent shear failure zone was localized as if it extended away from the hole as a continuation of the prominent shear zones. Specifically, a less prominent shear zone extended from the upper right wall of the hole and downward and to the right until it met the right boundary. Another less prominent shear zone extended from the lower left wall of the hole and upward and to the left until it met the left boundary. Figure 6D shows that tensile failures occurred within the localized shear zones, but also extended from these zones, mostly in the direction perpendicular to the direction of tension. Figure 6F shows the proximity of areas of tension to zones that had yielded in tensile mode, indicating a potential for further tensile yielding with additional far-field shearing.

PFC^{2D} will be used in the future to conduct these experiments and compare results with those of the FLAC models. Before proceeding, however, tests must be conducted to match particle contact and bond properties to elastic and strength properties of the FLAC continuum material. In the meantime, a preliminary experiment was run to examine capabilities.

A 4-m- (13-ft-) diameter hole was cut in a 12- by 12-m (39- by 39-ft) plate during the construction phase. Outside boundary walls were moved automatically as if in a servo-controlled test machine until the average stress on each wall was 6 MPa (870 psi). Next, the upper and lower walls were moved inward until the average stress was 205.6 MPa (29,820 psi). Average confining pressure was maintained at 6 MPa (870 psi). Figure 7 shows the expected system of diagonal cracks that intersected the hole from the upper left to the lower right. A companion fracture system appears to be developing at the lower left and upper right corners. These results are similar to results obtained by Fakhimi et al. (2002) in both their physical experiment and a numerical simulation with PFC^{2D}.

In a subsequent run of the model, vertical stress was only applied to 143.9 MPa (20,870 psi), while average stress on the sidewalls was maintained at 6 MPa (870 psi). At this stage, bond failures had not begun. Finally, the upper and lower walls were slowly rotated clockwise about their midpoints until displacement at the corners was 12.5 cm. Figure 8A shows a tensile crack extending from about 1:30 (as seen on a clock) upward and a little to the right. Failure zones of shear and tension begin around 4:00 and 10:00 and extend upward and to the right on the right side of the model and downward and to the left on the left side of the model. On the right side, the failure zone was not continuous, but a bridge formed between fracture zones where loading was able to continue (see figure 8B)

Rectangular Opening Experiment

This experiment was designed to examine the effects of mining a rectangular opening under conditions of preexisting shear stress caused by far-field shear. First a model was constructed with FLAC without far-field shear stress as a control. Vertical and horizontal compressive stresses of 41.37 and 20.68 MPa (6,000 and 3,000 psi), respectively, were applied at the bound-

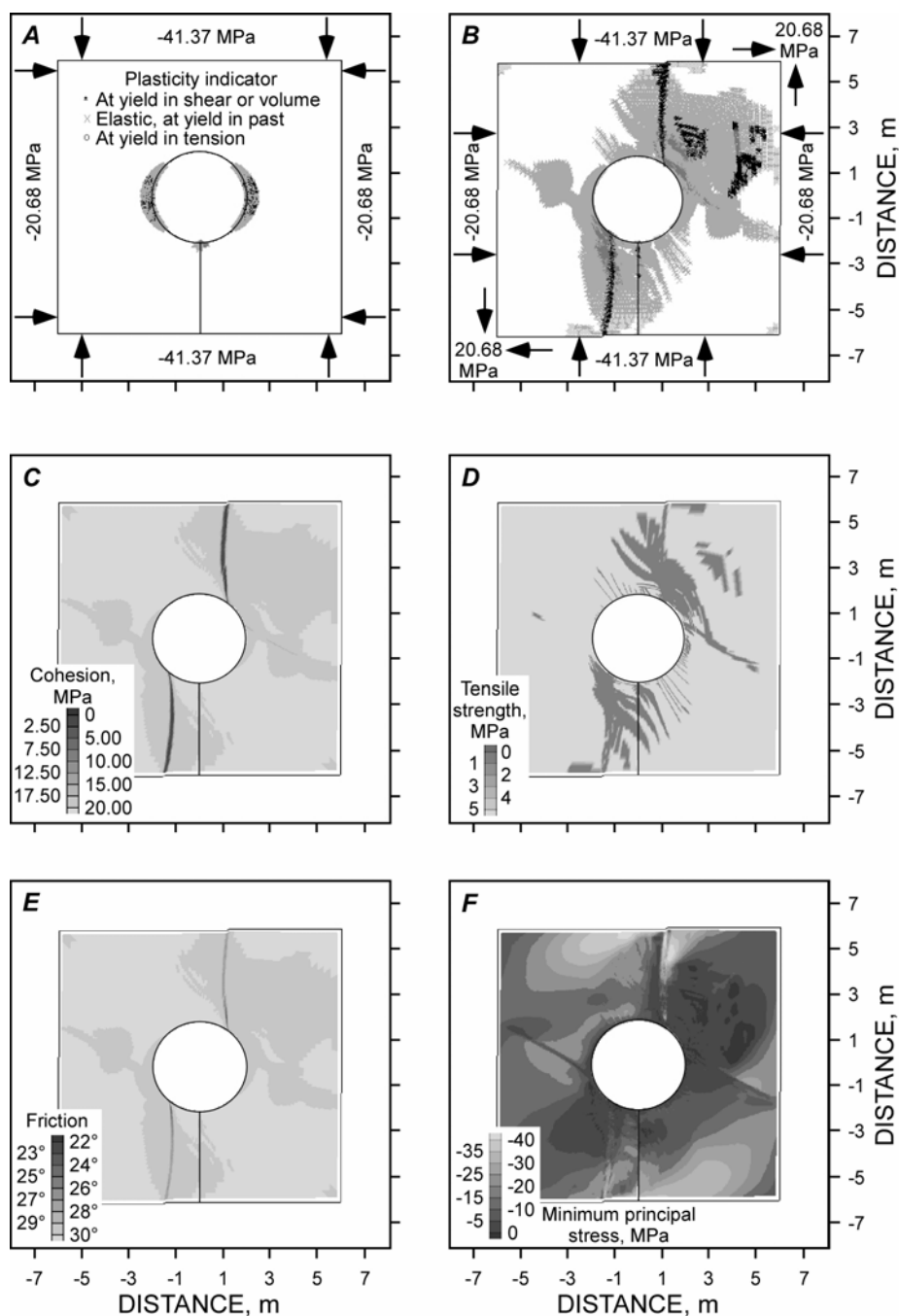


Figure 6.—Results of hole-in-a-plate experiment with shear stress applied to boundaries. *A*, Yield state of each element before application of boundary shear stress; *B*, yield state of each element after application of boundary shear stress; *C*, contours of cohesive strength showing location of cohesive softening; *D*, contours of tensile strength showing location of tensile softening; *E*, contours of friction angle showing location of friction softening; *F*, contours of minimum principal stress showing location of tensile zones. Boundary conditions shown in *B* apply also to *C*, *D*, *E*, and *F*.

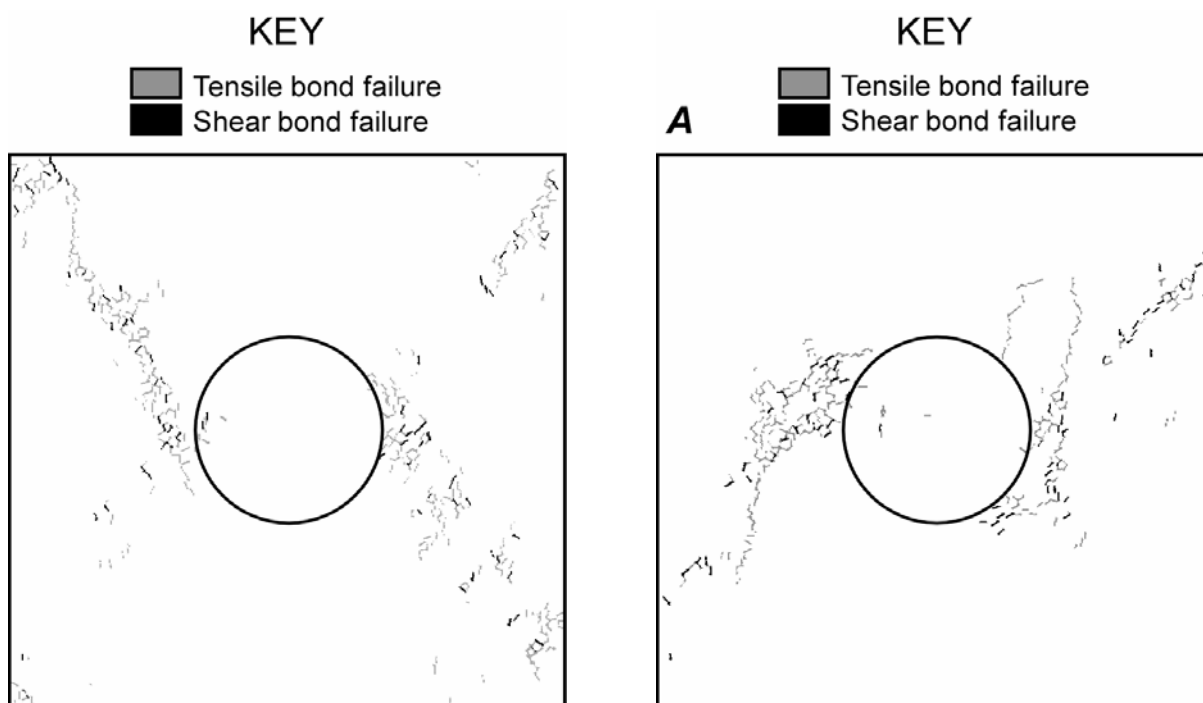


Figure 7.—Hole-in-a-plate experiment with horizontal confining and vertical deviatoric stress showing bond breakage according to failure mode.

aries and initialized in every element. The strain softening constitutive law with the same softening functions used in the hole-in-a-plate problem (figure 5) was incorporated into the model. A 6.1-by 4.3-m- (20- by 14-ft) opening was excavated in five stages to minimize the shock of removing confining forces suddenly. A nonlocal continuum model was not used because elements were small (7.62 by 7.62 cm [3 by 3 in]).

Figure 9 shows results of that model. Each stage of excavation produced a successively larger excavation, which is a reasonable approximation of a typical blasting sequence. Failure in shear extended from near the corner of each opening at a 45° angle to the roof and ribs, with the greater amount of failure extending into the ribs (figure 9A). Cohesion and friction softening coincided with the zone of shear (figure 9B and D) and also indicated previous softening from earlier excavation stages of the same shape. Tensile failures extended from these shear failure zones, primarily

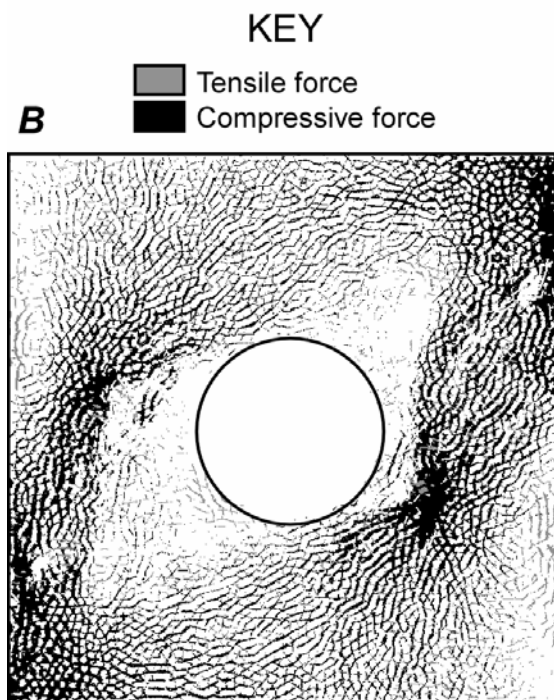


Figure 8.—Particle bond breakage resulting from far-field shear in hole-in-a-plate experiment. A, Bond breakage by mode of failure; B, contact forces.

Figure 8.—Particle bond breakage resulting from far-field shear in hole-in-a-plate experiment. A, Bond breakage by mode of failure; B, contact forces.

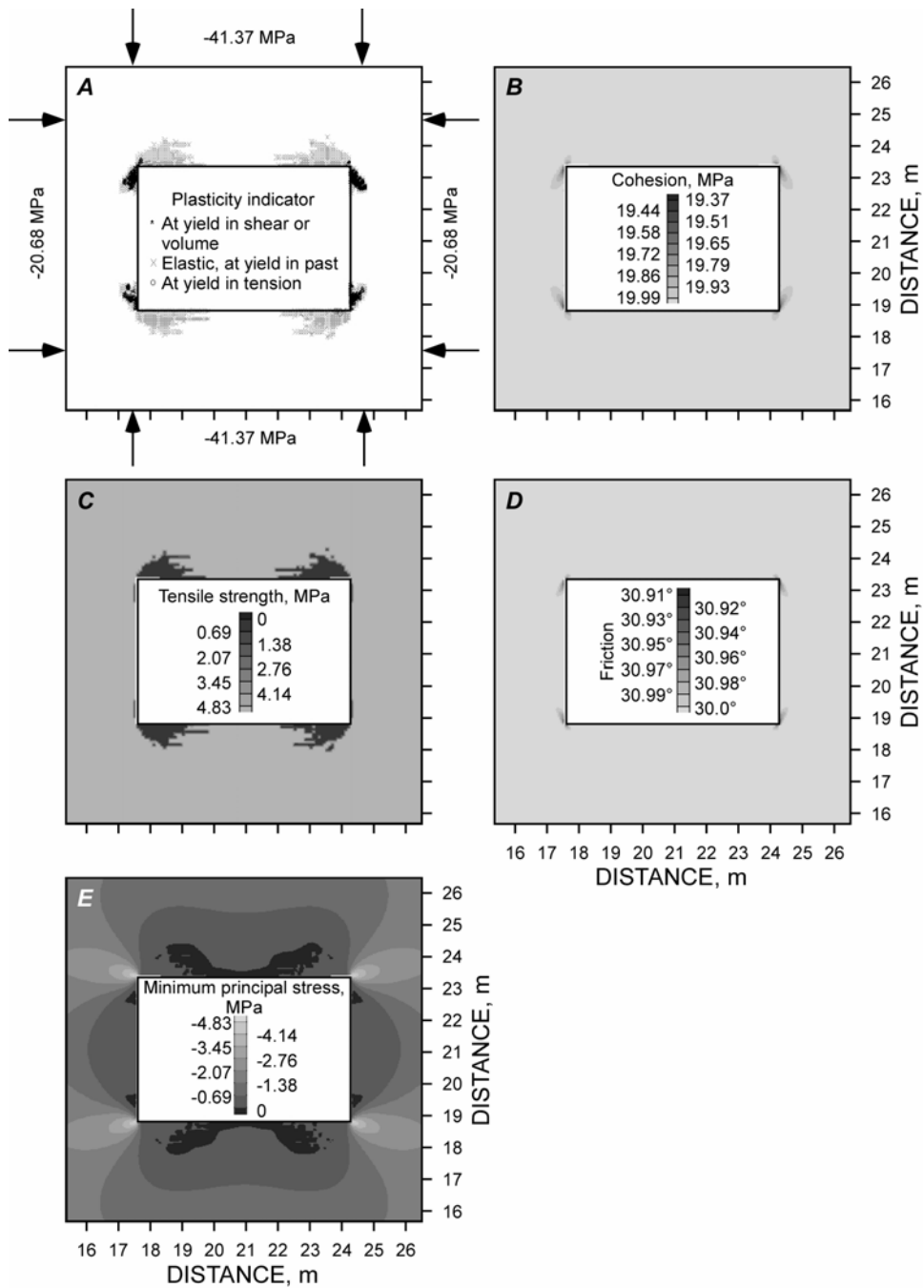


Figure 9.—Results of rectangular-opening model with no far-field application of shear stress. *A*, Yield state of each element; *B*, contours of cohesive strength showing location of cohesive softening; *C*, contours of tensile strength showing location of tensile softening; *D*, contours of friction angle showing location of friction softening; *E*, contours of minimum principal stress showing location of tensile zones. Boundary conditions shown in *A* also apply to *B*, *C*, *D*, and *E*

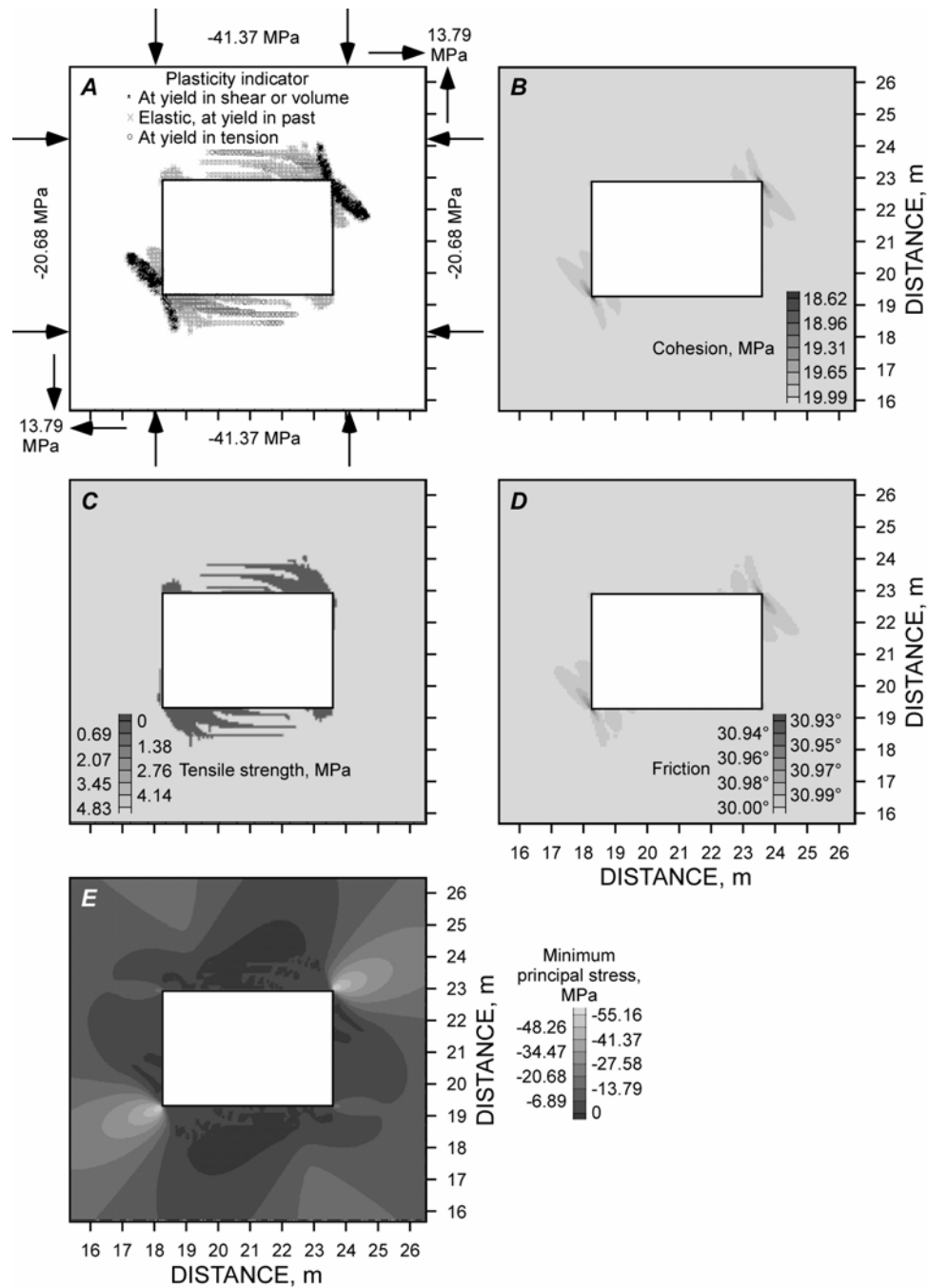


Figure 10.— Results of rectangular-opening FLAC model with far-field application of shear stress. *A*, Yield state of each element; *B*, contours of cohesive strength showing location of cohesive softening; *C*, contours of tensile strength showing location of tensile softening; *D*, contours of friction angle showing location of friction softening; *E*, contours of minimum principal stress showing location of tensile zones. Boundary conditions shown in *A* also apply to *B*, *C*, *D*, and *E*.

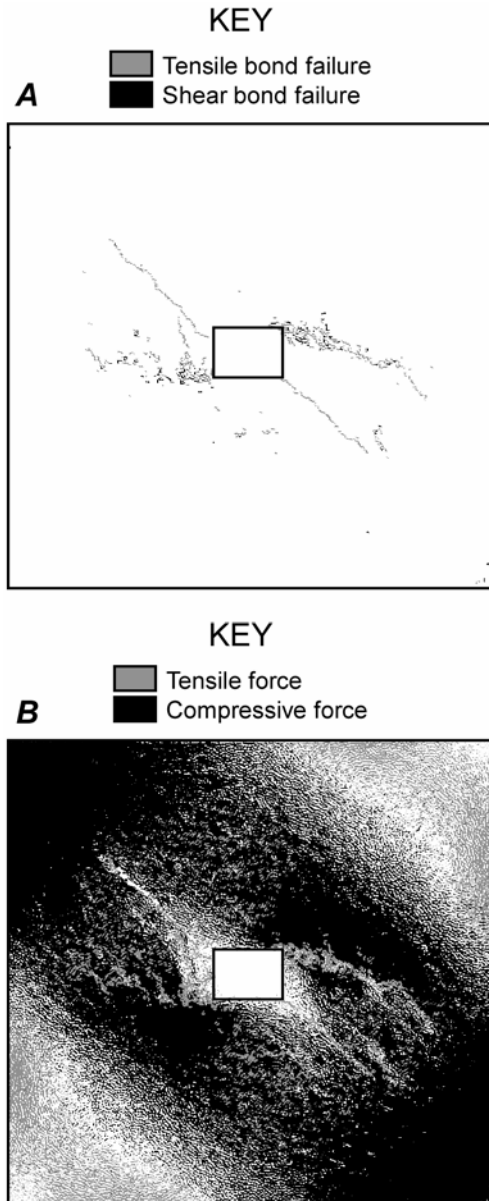


Figure 11.—Results of PFC^{2D} model with rectangular opening. A, Parallel bond breakage according to tensile and shear modes of failure; B, contact forces, both compressive and tensile.

shows bond-breakage results of the PFC^{2D} model. A tensile crack set originated near the upper left and lower right corners and extended diagonally at 45° to the roof line. These tensile cracks were absent in the FLAC model, but differences should be expected when boundary conditions, strengths, and stiffness of the material are not matched between FLAC and PFC^{2D} models. Additional zones in which bonds broke in both tensile and shear modes appeared near the lower left and upper right corners and extended away from the opening just above horizontal on the left and below horizontal on the right. Moreover, within these zones, one can see possible en echelon

above and below the openings, but not intersecting, as indicated in figure 9C. However, the minimum principal stress was tensile adjacent to the tensile failure zones, indicating the potential for further failure if more deviatoric stress were to be applied (figure 9E).

The model was rerun in FLAC with the same applied vertical and horizontal stresses. A shear stress of 13.79 MPa (2,000 psi) was applied at the boundaries and initialized in every element before excavation. Figure 10 shows results of the model. Instead of symmetrical shear zones at each corner of the opening, shear failure zones extended from opposite corners in roughly the same shape as appeared in the hole-in-a-plate model (figure 10A). However, the shear zones did not extend as far from the opening, probably because the boundaries were farther away (18.3 m [60 ft]), and the amount of applied shear stress was lower than in the hole-in-a-plate model. Also, the shear zones seem more prominent in the rib rather than above and below the opening (figures 10A, B, and D). Tensile failure zones took off from the shear zones, running largely parallel with the opening (figure 10C). Figure 10E shows tensile zones adjacent to tensile failure zones, suggesting the probable extension of tensile zones with further shear loading.

A PFC^{2D} model of the rectangular opening was constructed without first matching particle and bond properties and bond strengths to the FLAC continuum material. Applied horizontal and vertical stresses were 68.9 and 34.5 MPa (10,000 and 5,000 psi), respectively. The opening dimensions and distance to boundaries matched the FLAC model.

The left and right boundaries were rotated clockwise 22 cm (8.66 in) maximum at the corners, at which point fracture patterns were well developed for the level of parallel bond strength used (200 MPa [29,000 psi] with a standard deviation of 0.5 MPa [73 psi]). Figure 11A

distribution of bond breakage, though such formation is not clear. Given the small number of bond breakages directly above and below the opening, it is not hard to imagine further extension of the shear/tensile fractures angling over and below the openings from the existing shear/tensile crack set. Figure 11B shows contact forces. The location of tension and the contrast between much compressive force and little compressive force indicate the potential for shear/tensile crack extension above and below the opening.

DISCUSSION

The foregoing experiments had a few minor deficiencies. The far-field boundaries of the hole-in-a-plate model were too close to the opening so that boundary effects around the hole were not eliminated. The PFC^{2D} particle stiffnesses and bond strengths were not calibrated to FLAC models having selected elastic and strength properties so that model conditions would be similar. Far-field shear stresses were not applied in the same way as in the FLAC models. Therefore, the PFC^{2D} model results only illustrate capabilities.

The PFC^{2D} model results (figures 7 and 8) suggest that an echelon fracturing might be simulated, but careful tests must verify this suggestion. It appears from figure 8 that FLAC models are not likely to reflect distinct echelon fractures, but rather will localize failure to a narrow band in which both shear and tensile failures occur. These bands can be considered either a coalescence of microcracks or regions of echelon fractures.

Softening appears to be a reasonable way to represent fracturing with a FLAC model. However, one could argue that fractures could be better simulated if cohesion loss proceeded more quickly upon yielding—perhaps as quickly as the tension loss.

The presence of far-field shear stress caused preferential fracturing or yielding. Instead of the symmetrical yielding seen in figure 9, shear and tensile fracturing or yielding originated at two opposite corners of a rectangular opening instead of from all four corners. Similar localized shear zones appear both in the hole-in-a-plate model and the rectangular opening model, but the direction of prominent shear failure seemed to be affected by the shape of the rectangular opening when compared to shear failure around the circular opening. Examination of previous modeling results suggests that the applied horizontal-to-vertical stress ratio may also have an effect on the direction of prominent shear failure.

CONCLUSIONS

Far-field shear stress causes failure or yielding in preferential directions. Fracturing is no longer symmetrical around an underground opening. The results of the model experiments may not always directly relate to echelon fracturing, but relevant features are present, such as a fracture zone propagating over and under an opening at an acute angle to the surface. Therefore, the results are likely to be relevant to zones containing echelon sets of fractures. The models suggest the presence of both tensile and shear fracturing, although the FLAC model suggests that those zones may be adjacent to each other around a rectangular opening. Shape of the opening

and direction of far-field major and minor principal stresses appear to affect the direction of prominent shear failure, but more tests need to be conducted to assess cause and effect accurately.

REFERENCES

Bazant, Z.P., and G. Pijaudier-Cabot. 1987. Measurement of characteristic length of non-local continuum. Report 87-12/498m, Center for Concrete and Geomaterials, Northwestern University.

Bazant, Z.P., and G. Pijaudier-Cabot. 1988. Non-local continuum damage, localization instability and convergence. *J. Appl. Mech.*, V. 55, pp. 287-293.

Diederichs, M.S. 2002. Stress-induced damage accumulation and implications for hard rock engineering. In *Mining and Tunnelling Innovation and Opportunity, NARMS-TAC 2002*, Hammah et al. (eds.). Toronto: University of Toronto, V. 1, pp. 3-12.

Fakhimi, A., and C. Fairhurst. 1994. A model for the time-dependent behavior of rock. *Int. J. Rock Mech. Min. Sci. & Geomech. Abstr.*, V. 31, No. 2, pp. 117-126.

Fakhimi, A., F. Carvalho, T. Ishida, and J.F. Labuz. 2002. Simulation of failure around a circular opening in rock. *Int. J. Rock Mech. Min. Sci.*, V. 39, No. 4, pp. 507-515.

Fairhurst, C., and N.G.W. Cook. 1966. The phenomenon of rock splitting parallel to the direction of maximum compression in the neighborhood of a surface. In *Proceedings of the First Congress on the International Society of Rock Mechanics*, (Lisbon, Portugal, Sept. 25-Oct 1, 1966). Lisbon, Portugal: Nat. Lab. of Civil Eng., V. 1, pp. 687-692.

Itasca Consulting Group, Inc. (Minneapolis, MN). 1993. Fast Lagrangian Analysis of Continua (FLAC), User's Manual.

Itasca Consulting Group, Inc. (Minneapolis, MN). 1999. PFC^{2D} Particle Flow Code in 2 Dimensions, User's Guide.

Larson, M.K., C.L. Stewart, M.A. Stevenson, M.E. King, and S.P. Signer. 1995. A case study of a deformation mechanism around a two-entry gate road system involving probable time-dependent behavior. In *Proceedings of the Fourteenth International Conference on Ground Control in Mining*, S. Peng (ed.) (Morgantown, WV, Aug 1-3, 1995). Morgantown, WV: West Virginia University, pp. 295-304.

Larson, M.K., and H. Maleki. 1996. Geotechnical factors influencing a time-dependent deformation mechanism around an entry in a dipping seam. In *Proceedings of the Fifteenth International Conference on Ground Control in Mining*, Ozdemir, L., K. Hanna, K.Y. Harnam, and S. Peng (eds.), (Golden, CO, Aug 13-15, 1996). Golden, CO: Colorado School of Mines, pp. 699-710.

Larson, M.K.. 2003. *Time-dependent deformation and shear strength along weakness planes in the roof of a coal mine*. Ph.D. Thesis, University of Minnesota, 238 pp.

Peng, S.S., and A.M.Johnson, 1972. Crack growth and faulting in cylindrical specimens of Chelmsford granite. *Int. J. Rock Mech. Min. Sci.*, V. 9, pp. 37-86.

Rice, J.R. 1976. The localization of plastic deformation. In *Theoretical and Applied Mechanics*. W.T. Koiter (ed.). Amsterdam: North-Holland, pp. 202-220.

Terrill, L.J. and J.D. VandeKraats. 1997. Case study of conditions observed during the removal of a highly fractured roof beam in bedded halite. In *Proceedings, 16th Conference on Ground Control in Mining*, S. Peng (ed.) (Morgantown, WV, Aug. 5-7, 1997). Morgantown, WV: West Virginia University, pp. 235-242.

White B.G. 2002. Shear mechanism for mining-induced fractures applied to rock mechanics of coal mines. In *Proceedings, 21st International Conference on Ground Control in Mining*, S. Peng, C. Mark, A.W. Khair, and K. Heasley (eds.) (Morgantown, WV, Aug. 6-8, 2002). Morgantown, WV: West Virginia University, pp. 328-334.

White, B., S. Iverson, and M. Larson. 2003. Shear origin of tension in excavation-induced fractures, In *Proceedings for Soil and Rock America 2003 and 39th Rock Mechanics Symposium*, P. J Culligan, H. H. Einstein, and A. J. Whittle (eds.) V. 1, pp. 909-916.

White, B.G., M. Larson, and S.R. Iverson. Origin of mining-induced fractures through macroscale distortion. In press. *Gulf Rocks 2004: Rock Mechanics Across Borders and Disciplines, 6th North American Rock Mechanics Symposium* (Houston, TX, June 5-10, 2004).

Zietlow, W.K., and J.F. Labuz. 1998. Measurement of the intrinsic process zone in rock using acoustic emission. *Int. J. Rock Mech. Min. Sci.*, V. 35, No. 3, pp. 291-299.